# A multi-resolution particle/fluctuating hydrodynamics model for hybrid simulations of liquids based on the two-phase flow analogy

*J. Hu,*[1] *I.A. Korotkin,*[1] *S.A. Karabasov*[1]

[1]*The School of Engineering and Materials Science, Queen Mary University of London, Mile End Road, E1 4NS London, United Kingdom*

## Abstract

A triple-scale model of a molecular liquid, where atomistic, coarse-grained, and hydrodynamic descriptions of the same substance are consistently combined, is developed. Following the two-phase analogy method, the continuum and discrete particle representations of the same substance are coupled together in the framework of conservation laws for mass and momentum that are treated as effective phases of a nominally two-phase flow. The effective phase distribution, which governs the model resolution locally, is a user defined function. In comparison with the previous models of this kind in the literature which used the classical Molecular Dynamics (MD) for the particulate phase, the current approach uses the Adaptive Resolution Scheme (AdResS) and stochastic integration to smoothen the particle transition from non-bonded atom dynamics to hydrodynamics. Accuracy and robustness of the new AdResS-Fluctuating Hydrodynamics (FH) model for water at equilibrium conditions is compared with the previous implementation of the two-phase analogy model based on the MD-FH method. To demonstrate that the AdResS-FH method can accurately support hydrodynamic fluctuations of mass and momentum, a test problem of high-frequency acoustic wave

propagation through a small hybrid computational domain region is considered.

**Key words**: multi-scale modelling, molecular dynamics, soft matter, non-bonded interactions, coarse-graining, AdResS, two-phase flow analogy

## 1. Introduction

One of the most accurate simulations methods, which provides detailed information at the atomistic level is Molecular Dynamics (MD) that solves Newtonian equations of motion by computing the inter-particle forces. For non-bonded interactions typical of soft matter dynamics, clusters of particles can freely move, and the relevant length scale of the system in space and time can be very large compared to the interatomic distance. In such systems, the number of Degrees Of Freedom (DOFs) which corresponds to all-atom MD simulations quickly become prohibitively expensive [1]. In this case, some accuracy sacrifices need to be made to reduce the total number of DOFs in the simulation to an affordable level. For example, the standard solution in case all-atom details are not crucial is based on the concept of Coarse Graining (CG). Here, several atoms are regarded as one effective particle governed by some effective force potential at the mesoscopic level. For simulating even larger particle systems in space and time scales, the CG particles can be further agglomerated into macroscopic particles and the unresolved thermal fluctuations interactions are modeled statistically using Dissipative Particle Dynamics and Fluctuating Hydrodynamics models [2], [3]. Furthermore, for very large space and time scales relevant for Navier-Stokes hydrodynamics, using

constitutive equations derived at the microscopic level, macroscopic particles can be further integrated into discrete Lagrangian parcels of fluids using Smooth Particle Hydrodynamics (SPH) [4], [5] or Lattice Boltzmann Method (LBM) [6], [7] as well as represented on the Eulerian grid using finite-difference (FD), finite-volume (FV), and finite-element (FE) methods available [8]–[11].

In other applications, such as of interest in the current publication, the all-atom resolution is required in a certain small part of the computational domain, while the rest of the domain can be simulated with the use of continuum hydrodynamics methods. The multi-resolution simulations are challenging as they require coupling of the models which correspond to very different number of DOFs.

Since the 1990s, various attempts to couple the molecular dynamics and continuum hydrodynamics (CH) started to appear in the multiscale literature [12], [13]. In many approaches, the fine-scale MD model is connected to continuum models by a continuum-atomistic overlap region which acts as a boundary separating the two sub-domains of different resolution. For the overlap region, state variables schemes and flux coupling schemes are introduced. In the state variables schemes [12], [14], [15], [16], the connection interface between the MD and CH regions is solved by a finite zone that keeps the conservation of bulk mass and momentum fluxes. In the flux coupling schemes, a control interface is used to exchange the conservation fluxes between the hydrodynamic and atomistic parts of the solution [3]. It was shown that it is important for the multiscale model to satisfy macroscopic conservation laws such as mass and linear momentum as well as to have a model preventing the artificial phase separation

between the zones of different resolutions which correspond to different free energies. Additionally, the all-atom resolution and the continuum part of the model should be smoothly connected so that the particles at all-atom resolution gradually transition to large continuum scales. In particular, a finite overlap region between MD and hydrodynamic part of the solution is needed to avoid artefacts such as sharp oscillations in density and pressure between different representations of the same chemical substance [17].

In [18] and [19], a sophisticated two-phase flow analogy method for smoothly coupling the Landau and Lifshitz Fluctuating Hydrodynamics equations (LL-FH) with MD was developed. By introducing an atomistic particle and a continuum representation of the same liquid, the method was formulated as mass and momentum equations of a nominally two-phase flow where the concentration of each phase is a user-defined function. To avoid the artificial phase separation and preserve the continuity of variances of macroscopic flow quantities across the different phases, forcing terms were introduced as sources and sinks in the nominally two-phase equations without affecting the conservation of mass and momentum fluxes.

Still, performance of even most sophisticated multiscale methods where a fully continuum flow model is directly coupled to molecular dynamics becomes rather sensitive to the implementation details in the unsteady cases where no complete scale separation can be assumed. The reason for this sensitivity is a too rapid change which particles must undergo on their way from non-bonded molecular dynamics to constrained particles, which are driven by the continuum Navier-Stokes or Fluctuating

Hydrodynamics equations. The rapid change may lead to a too close distance between the adjacent atoms which, in turn, generates large inter-atomic forces making the system to depart from the correct equilibrium conditions.

To reduce the sensitivity, the concept of particle scale bridging with a gradual transition from a large number of DOFs (atoms) to a reduced number of DOFs (coarse grained particles) was introduced and implemented in the Adaptive Resolution Scheme (AdResS), [17]. The idea of AdResS is to introduce a smooth coupling of particles at different resolutions by preserving mass and linear momentum by using a force interpolation scheme. Subsequently, a particle sorting algorithm based on the energy minimisation (USHER [20]) is introduced for inserting particles in the hydrodynamic region. This method is used in the subsequent work [21], where a concurrent triple scale model was introduced that combines the AdResS with Navier-Stokes equations through a hybrid molecular-continuum hydrodynamics scheme (Hybrid MD). The Hybrid MD is based around the idea of the momentum flux exchange between the MD and the Navier-Stokes model at the hybrid interface *H* for the conservation of mass and momentum fluxes, apart from the additional buffer domain *B*, which is needed to operate *H* smoothly. *B* is a mass and momentum reservoir of the particles and used for imposing the external momentum into the molecular dynamic region.

Because of the flux coupling scheme, the concurrent AdResS-Hybrid MD method treats the multi-scale particle AdResS part and the continuum Navier-Stokes part as two different fields separated by interface. This interface together with the reservoir *B* play the role of an artificial boundary between the two very different representations of the

same chemical substance: the models can inform one another in terms of the transport coefficients and other macroscopic properties but remain very different conceptually. This separation may not be ideal from the viewpoint of a sufficiently smooth transition from one part of the multiscale model to the other.

On the other hand, the idea of using the two-phase analogy [18] for coupling the continuum and discrete representations of the same liquid, which doesn't require additional adjustments, such as an artificial particle reservoir, appears to be an attractive alternative to the existing triple-scale AdResS method based on the flux coupling scheme. The current paper is the first step in developing an alternative AdResS-Hybrid MD formulation that is based on the two-phase analogy where the multi-resolution particles from the AdResS phase interact with the Fluctuating Hydrodynamics equations in accordance with the governing equations of conservation of mass and momentum of the two-phase mixture.

The paper is organised as the following. In the theory part (section 2), the two-phase analogy for modelling of liquids at multiple resolution and its simplified one-way coupling implementation, which assumes no significant feedback of the particulate phase on the dynamics of the entire liquid, are briefly reviewed in subsections 2.1 and subsection 2.2, respectively, and the AdResS method for multi-resolution particle simulations is outlined in subsection 2.3. In subsection 2.4, the new coupling scheme between AdResS and Fluctuating Hydrodynamics, which uses the two-phase analogy approach, is presented as a generalisation of the stochastic Verlet-type integration scheme for coarse-grained particle dynamics, where the inter-particle force is calculated

with the AdResS method. Numerical results of the new triple scale AdResS–FH model and their comparison with the solutions of the previous hybrid MD-FH model are presented in Section 3.

## 2. Theory

### 2.1 Two-phase analogy for coupling continuum and particle representations of the same liquid

The hybrid two-phase analogy model for multi-resolution simulations of liquids [18] is briefly summarised below.

Large-scale continuum and fine-scale particle representations of the same chemical substance are considered as the 'phases' of the same nominally two-phase fluid. The concentration of the particle phase and the continuum phase are $0 \le s \le 1$ and $0 \le 1\text{-}s \le 1$, respectively, where $s$ is a user-defined function of space and time that describes which part of the volume is represented by discrete particles and which by continuum. The process of phase mixing, which corresponds to changing the model resolution, is specified by user-defined sources in the corresponding two-phase equations of conservation of mass and momentum. Under assumption that there is no macroscopic temperature gradients, the macroscopic temperature equation is irrelevant, and the corresponding conservation equations of mass of the continuum phase

$$\delta_t(sm) + \sum_{\gamma=1,6} (s\rho\bar{\mathbf{u}}) d\mathbf{n}^{\gamma} \delta t = \delta_t J^{(\rho)} \tag{1}$$

the equation of mass of the particle phase

$$\delta_t\left((1-s)\sum_{p=1,N(t)} m_p\right)+\sum_{\gamma=1,6}\left((1-s)\sum_{p=1,N_\gamma(t)}\rho_p\mathbf{u}_p\right)d\mathbf{n}^\gamma\delta t=-\delta_t J^{(\rho)}, \tag{2}$$

the equation of momentum of the continuum phase

$$\delta_t(smu_i)+\sum_{\gamma=1,6}\left(s\rho u_i\bar{\mathbf{u}}\right)d\mathbf{n}^\gamma\delta t=s\sum_{j=1,3}\sum_{\gamma=1,6}\left(\Pi_{ij}+\tilde{\Pi}_{ij}\right)dn_j^\gamma\delta t+\delta_t J_i^{(\mathbf{u})}, \tag{3}$$

and that of momentum of the particle phase

$$\delta_t\left((1-s)\sum_{p=1,N(t)} m_p u_{ip}\right)+\sum_{\lambda=1,6}\left((1-s)\sum_{p=1,N_\gamma(t)}\rho_p u_{ip}\mathbf{u}_p\right)d\mathbf{n}^\gamma\delta t=(1-s)\sum_{p=1,N(t)}F_{ip}\delta t-\delta_t J_i^{(\mathbf{u})}, \tag{4}$$

are formulated on a Eulerian grid of hexahedral control volumes, $V$.

Here the fields which correspond to the particles are with a sub-index $p$ and those which stand for the cell-volume averaged and the cell-flux averaged quantities (e.g. obtained from an appropriate reconstruction inside each cell in accordance with a finite-volume method) are without the sub-index. $\gamma=1,..,6$ are the faces of each hexagonal-type control volume, $m$ and $\rho=m/V$ are the mass and density of the continuum phase of the elementary volume, $m_p$ is the particle mass, $\mathbf{u}_p$ is the particle velocity, $\bar{\mathbf{u}}$ is the particle-continuum 'mixture' velocity, $\bar{u}_i=\left[s\rho u_i+(1-s)\sum_{p=1,N(t)}\rho_p u_{ip}\right]/\bar{\rho}$, $u_i$ is the velocity of the continuum LL-FH phase, $\bar{\rho}$ is the mixture density, $\bar{\rho}=s\rho+(1-s)\sum_{p=1,N(t)}\rho_p$, $N(t)$ is the number of particles in the volume $V$. $N_\gamma(t)$ is the number of particles crossing the $\gamma^{th}$ cell face with the area normal $d\mathbf{n}^\gamma$ at time $t$, $\rho_p=m_p/V$ is the effective density of particle $p$ per volume $V$, $\delta_t$ describes the change of each quantity over time $\delta t$, e.g. counts the particle mass and momentum accumulated in cell $V$ over time $\delta t$. $F_{ip}$ is the total inter-particle interaction force exerted on particle $p$.

For the continuum phase momentum equation, the Landau-Lifshitz Fluctuating

Hydrodynamics model is used, which is implemented by adding the random stress tensor, $\tilde{\boldsymbol{\Pi}}$ to the deterministic stress of the Navier-Stokes equations, $\boldsymbol{\Pi}$ in order to account for the effect of Brownian motion. $\delta_t J^{(\rho)}$ and $\delta_t J_i^{(\mathbf{u})}$ are the mass and the momentum exchange terms between the two phases, which are a function of the user-defined phase concentration function $s$. These exchange terms control how fast the fine-scale particle phase ($s = 0$) is replaced by the large-scale continuum phase ($s = 1$) in the computational domain to strike a balance between the computational cost reduction and accuracy.

Important properties of the system of conservation laws (1)-(4) include conservation of mass $\bar{m} = \bar{\rho}V$ and momentum fluxes in accordance with Newton's second law that equates the change of the total momentum $\bar{m} \cdot \bar{\mathbf{u}}$ to the force applied, $\bar{F}_i = s \sum_{j=1,3} \sum_{\alpha=1,6} \left( \Pi_{ij} + \tilde{\Pi}_{ij} \right) dn_j^{\alpha} \delta t + (1-s) \sum_{p=1,N(t)} F_{ip}$.

The two-phase analogy model is closed by defining the particle-particle interaction model (e.g. in accordance with classical Molecular Dynamics) and introducing the appropriate continuum-discrete source fields in the kinematic and dynamic equation for each particle so that, collectively, the particle phase satisfies the governing conservation laws (1)-(4).

### 2.2 A single-resolution particle liquid in the fluctuating hydrodynamics bath

Following the assumptions considered in [19], the effect of discrete particles on the macroscopic hydrodynamics is ignored, and the dependent variables of the hybrid two-

phase mixture, $\overline{\rho}$ and $\overline{u}_i$ are replaced by the solution of the Landau-Lifshitz – Fluctuating Hydrodynamics (LL-FH) model that represents the statistical properties of liquids at mesoscale:

$$\begin{aligned} &\frac{\partial \overline{\rho}}{\partial t} + div\left(\overline{\rho}\cdot\overline{\mathbf{u}}\right) = 0, \\ &\frac{\partial\left(\overline{\rho}\cdot\overline{u}_i\right)}{\partial t} + div\left(\overline{\rho}\cdot\overline{u}_i\cdot\overline{\mathbf{u}}\right) = \sum_{j=1,3} \nabla_j\left(\Pi_{ij} + \tilde{\Pi}_{ij}\right),\ i=1,2,3 \end{aligned} \tag{5}$$

Here $\overline{p} = \overline{p}(\overline{\rho})$ in accordance with the equation of state, the stress tensor $\mathbf{\Pi}$ and its fluctuating component $\tilde{\mathbf{\Pi}}$ are defined so that

$$\begin{aligned} &\Pi_{i,j} = -\left(\overline{p} - \zeta div\,\overline{\mathbf{u}}\right)\delta_{i,j} + \eta\left(\partial_i\overline{u}_j + \partial_i\overline{u}_j - 2D^{-1}div\,\overline{\mathbf{u}}\delta_{i,j}\right), \\ &\tilde{\Pi}_{i,j} = \zeta div\,\tilde{\mathbf{u}}\delta_{i,j} + \eta\left(\partial_i\tilde{u}_j + \partial_i\tilde{u}_j - 2D^{-1}div\,\tilde{\mathbf{u}}\delta_{i,j}\right), \quad i,j=1,2,3 \end{aligned} \tag{6}$$

where $\eta$ and $\zeta$ are shear and bulk viscosity coefficients. $\tilde{\mathbf{\Pi}}$ is modelled as a random Gaussian matrix with zero mean and covariance:

$$\left\langle \tilde{\Pi}_{i,j}(\mathbf{r}_1,t_1)\tilde{\Pi}_{k,l}(\mathbf{r}_2,t_2)\right\rangle = 2k_BT\left[\eta\left(\delta_{i,k}\delta_{j,l}+\delta_{i,l}\delta_{j,k}\right)+\left(\zeta-2D^{-1}\eta\right)\delta_{i,j}\delta_{k,l}\right]\delta(t_1-t_2)\delta(\mathbf{r}_1-\mathbf{r}_2). \tag{7}$$

Following [22], the stochastic stress tensor is represented explicitly so that

$$\tilde{\Pi}_{i,j} \cong \sqrt{\frac{2k_BT}{\delta t\delta V}}\left(\sqrt{2}\sqrt{\eta}\cdot G^S_{i,j} + \sqrt{D}\sqrt{\zeta}\cdot tr\left[\mathbf{G}\right]\cdot E_{i,j}/D\right), \quad i,j=1,2,3 \tag{8}$$

where $\mathbf{G}$ is a random Gaussian matrix with zero mean and covariance $\left\langle G_{i,j}G_{k,l}\right\rangle = \delta_{i,j}\delta_{k,l}$, $G^S_{i,j} = \dfrac{G_{i,j}+G^T_{i,j}}{2} - tr[\mathbf{G}]\cdot E_{i,j}/D$, is a random symmetric matrix with zero trace, $\mathbf{E}$ is the identity matrix, and $tr\left[\mathbf{G}\right]$ is the trace of the matrix $\mathbf{G}$.

The above leads to the one-way coupled MD-FH model when the hydrodynamic equations (5)-(8) are solved with a central finite-volume method [23]. The FH solution provides an effective hydrodynamic "bath" where the particle are immersed in

accordance with the following equations for particle coordinates and velocities of Non-Equilibrium Molecular Dynamics (NEMD)-type:

$$
\begin{aligned}
&\frac{d\mathbf{x}_p}{dt} = \mathbf{u}_p + \mathbf{Q}_1, \\
&\frac{d\mathbf{u}_p}{dt} = \mathbf{Q}, \\
&\mathbf{Q}_1 = s(\bar{\mathbf{u}} - \mathbf{u}_p) + s(1-s)\cdot\alpha\cdot\frac{\sum_{\gamma=1,6}\left(\bar{\rho} - \sum_{q=1,N_\gamma(t)}\rho_q\right)d\mathbf{n}^\gamma}{\sum_{q=1,N(t)} m_q} \\
&Q_i = (1-s)F_{p,i}/m_p + \sum_{k=1,3}\sum_{\gamma=1,6}\left(s(1-s)\cdot\alpha\cdot\sum_{q=1,N_\gamma(t)}\rho_q u_{iq}\cdot\left(\frac{\sum_{\lambda=1,6}\left(\bar{\rho} - \sum_{q=1,N_\lambda(t)}\rho_q\right)dn_k^\lambda}{\sum_{q=1,N(t)} m_q}\right)\right)dn_k^\gamma / \sum_{q=1,N(t)} m_q \\
&+\sum_{k=1,3}\sum_{\gamma=1,6}\left(s(1-s)\cdot\beta\cdot\frac{1}{V}\left(\sum_{\lambda=1,6}\left(\bar{\rho}\cdot\bar{u}_i - \sum_{q=1,N_\lambda(t)}\rho_q u_{iq}\right)dn_k^\lambda\right)\right)dn_k^\gamma / \sum_{q=1,N(t)} m_q, \qquad i=1,2,3.
\end{aligned}
\tag{9}
$$

Here, the macroscopic fields correspond to control volume-averaged values and conservative fluxes are defined through the six sides of each control volume in accordance with the area normal $d\mathbf{n}^\gamma$, γ=1,..,6. All fields are interpolated to the current particle location. For simplicity, all functions inside the cell are reconstructed via a linear interpolation and the values of the fluxes are computed by interpolation in accordance with a central finite-volume scheme. $\alpha, \beta > 0$ are adjustable parameters that correspond to how fast the particle phase is forced to 'diffuse' to the Fluctuating Hydrodynamics solution in the hybrid region 0<s<1. In [19] and subsequent works [24], [25], the inter-particle forces, $F_{p,i}$ are defined in accordance with the classical Molecular Dynamics and Eq(9) is integrated with the standard velocity Verlet algorithm [26].

### 2.3 AdResS model

Compared to other molecular dynamics methods, the distinct feature of AdResS is that the number of high-resolution particles (atoms) is not fixed but can vary over the computational domain during the simulation time. In the coarse grained (CG) solution region, atoms are agglomerated into molecules which are modelled as single particles. For every molecule, a well-defined mapping point is used such as the center of mass or another linear combination of the internal particle coordinates. The forces in the coarse-grained region are functions of the mapping point positions only. The molecules are modelled by charge groups or sets of charge groups, which allows one to have multiple mapping points per molecule. The atomistic and coarse grained scales are coupled based on the potential derived from the reference all-atom molecular dynamic system by a position dependent interpolation equation [17]:

$$F_{\alpha\beta} = w(X_\alpha)w(X_\beta)F_{\alpha\beta}^{atom} + \left[1 - w(X_\alpha)w(X_\beta)\right]F_{\alpha\beta}^{cg},$$

The coupling scheme preserves linear momentum that is of importance for hydrodynamics. $\alpha$ and $\beta$ represent a pair of the two particles, $F_{\alpha\beta}^{atom}$ and $F_{\alpha\beta}^{cg}$ are the corresponding force potentials which represent the explicit interaction and coarse-grained interaction of the particles, respectively, and $w(X_\alpha)$, $w(X_\beta)$ stand for the weighting function:

$$w(x) = \begin{cases} 1, & \textit{atomistic region}; \\ 0 < w < 1, & \textit{hybrid region}; \\ 0, & \textit{coarse} - \textit{grained region.} \end{cases}$$

In comparison with the pure CG region, where the potential between the mapping points is generated by the static CG approach that reproduces the radial distribution function

of the molecular dynamics system as accurately as possible, in the AdResS system, the dynamic CG is implemented for the friction forces between the CG degrees of freedom. Additionally, an external force, the so-called thermodynamic force (TF) [27], is applied in the variable-resolution hybrid zone to reduce the local density inhomogeneities between the atomistic and coarse-graining representations and, thus, to enforce the continuity of pressure across the solution domain [28].

### 2.4 A multi-resolution particle liquid in the fluctuating hydrodynamics bath

In comparison with the all-atom simulations, in multi-resolution particle simulations one also needs to integrate the equations of motion of coarse-grained particles. The latter include the deterministic particle-particle interactions as well as contributions from the unresolved interactions modeled as random fluctuations balanced by velocity-dependent frictional forces to preserve the solution variance appropriately. Accordingly, the Newton's second law for particle motion is changed to the generalized Langevin equation:

$$\dot{\mathbf{u}}_p(t) = -\gamma \mathbf{u}_p(t) + \mathbf{Q}, \tag{10}$$

where $\mathbf{Q}=\mathbf{F}_p\left(\{\mathbf{x}(t)\}\right)/m_p + \mathbf{R}_p(t)/m_p$ , $\mathbf{F}_p$ is the deterministic pair-particle interaction force, and $\mathbf{R}_p$ represents the stochastic force, which is balanced by friction force with a suitably adjusted coefficient $\gamma$ to obtain the correct variance. The stochastic force $\mathbf{R}_p$ is a stationary Gaussian random variable with a zero mean that is assumed to be independent from the prior velocities and the deterministic force.

The stochastic Leapfrog integration scheme for coarse-grained particle dynamics was suggested in [29]. This approach will be used as a starting point for the current work, hence, it is briefly outlined below.

The development is based on approximating the analytical solution of the Langevin equation staggered at the whole and the mid time steps

$$\mathbf{u}_p(t+\Delta t) = \mathbf{u}_p(t)e^{-\gamma\Delta t} + e^{-\gamma\Delta t}\int_0^{\Delta t} e^{+\gamma\Delta t}\mathbf{Q}(t+t')dt' = \mathbf{u}_p(t)e^{-\gamma\Delta t} + \mathbf{Q}(t)\frac{1-e^{-\gamma\Delta t}}{\gamma} + H.O.T. \quad (11)$$

$$\mathbf{x}_p(t+\Delta t/2) = \mathbf{x}_p(t-\Delta t/2) + \int_{-\Delta t/2}^{\Delta t/2}\mathbf{u}_p(t+t')dt' = \mathbf{x}_p(t) + \mathbf{u}_p(t)\frac{e^{\gamma\Delta t/2} - e^{-\gamma\Delta t/2}}{\gamma} + H.O.T. \quad (12)$$

where $H.O.T.$ are high-order terms with respect to the integration time step,

so that at the first half step

$$\mathbf{u}_p(t+\frac{1}{2}\Delta t) = \mathbf{u}_p(t)\cdot e^{-\gamma\Delta t} + \frac{\mathbf{F}_p}{\gamma}(1-e^{-\gamma\Delta t}) + \{\mathfrak{R}_1\}, \quad (13)$$

$$\mathbf{x}_p(t+\frac{1}{2}\Delta t) = \mathbf{x}_p(t) + \frac{\mathbf{u}_p(t+\frac{1}{2}\Delta t)}{\gamma}(e^{\gamma\Delta t/2} - e^{-\gamma\Delta t/2}), \quad (14)$$

and at the second half step

$$\mathbf{u}_p(t+\Delta t) = \frac{\left(\mathbf{x}_p(t+\frac{1}{2}\Delta t) - \mathbf{x}_p(t)\right)\gamma}{e^{\gamma\Delta t/2} - e^{-\gamma\Delta t/2}} \equiv \mathbf{u}_p(t+\frac{1}{2}\Delta t), \quad (15)$$

$$\mathbf{x}_p(t+\Delta t) = \mathbf{x}_p(t+\frac{1}{2}\Delta t) + \{\mathfrak{R}_2\}, \quad (16)$$

where $\mathfrak{R}_1, \mathfrak{R}_2$ are stochastic excitation functions corresponding to unresolved particle dynamics interactions (comp. with $\mathbf{R}_p$ in Eq.(10)). Details for the stochastic excitation functions are given in Appendix for reference.

In the framework of the AdResS implementation [30], the stochastic excitation terms and the corresponding friction forces are switched to zero in the zone of all-atom molecular dynamics and are activated to the full in the coarse-grained particle region.

To obtain a multi-resolution particle AdReSs – Fluctuating Hydrodynamics (FH) scheme, the same stochastic integration technique is applied to solve Eq.(9).

First, by taking into account the Fluctuating Hydrodynamics bath, the first half step of the modified stochastic Leapfrog scheme becomes (comp. with Eqs.(13),(14))

$$\mathbf{u}_p(t+\frac{1}{2}\Delta t)=\mathbf{u}_p(t)\cdot e^{-\gamma\Delta t}+\frac{\mathbf{Q}}{\gamma}(1-e^{-\gamma\Delta t})+\{\mathfrak{R}_1\}, \qquad (17)$$

and

$$\mathbf{x}_p(t+\frac{1}{2}\Delta t)=\mathbf{x}_p(t)+\frac{\mathbf{u}^*}{\gamma}(e^{\gamma\Delta t/2}-e^{-\gamma\Delta t/2}), \qquad (18)$$

where the source term includes a contribution of the Fluctuating Hydrodynamics and the effect of the AdResS scheme is agglomerated in the particle forces $F_{p,i}$:

$$Q_i=(1-s)F_{p,i}/m_p-s\{\mathfrak{R}_{1,i}\}+\sum_{k=1,3}\sum_{\gamma=1,6}\left(s(1-s)\cdot\alpha\cdot\sum_{q=1,N_\gamma(t)}\rho_q u_{iq}\cdot\left(\frac{\sum_{\lambda=1,6}\left(\bar{\rho}-\sum_{q=1,N_\lambda(t)}\rho_q\right)dn_k^\lambda}{\sum_{q=1,N(t)}m_q}\right)\right)dn_k^\gamma/\sum_{q=1,N(t)}m_q$$

$$+\sum_{k=1,3}\sum_{\gamma=1,6}\left(s(1-s)\cdot\beta\cdot\frac{1}{V}\left(\sum_{\lambda=1,6}\left(\bar{\rho}\cdot\bar{u}_i-\sum_{q=1,N_\lambda(t)}\rho_q u_{iq}\right)dn_k^\lambda\right)\right)dn_k^\gamma/\sum_{q=1,N(t)}m_q, \qquad i=1,2,3.$$

and the effective velocity $\mathbf{u}^*$ of the particles includes the effect of the continuum hydrodynamics

$$\mathbf{u}^*=\mathbf{u}_p\left(t+\frac{1}{2}\Delta t\right)+\left(s\left(\bar{\mathbf{u}}-\mathbf{u}_p\left(t+\frac{1}{2}\Delta t\right)\right)+s(1-s)\cdot\alpha\cdot\frac{\sum_{\gamma=1,6}\left(\bar{\rho}-\sum_{q=1,N_\gamma(t)}\rho_q\right)d\mathbf{n}^\gamma}{\sum_{q=1,N(t)}m_q}\right)$$

For the second half step, the modified stochastic Leapfrog scheme is (comp. with Eqs. (15),(16)):

$$\mathbf{u}_p(t+\Delta t)=\frac{\left(\mathbf{x}_p(t+\frac{1}{2}\Delta t)-\mathbf{x}_p(t)\right)\gamma}{e^{\gamma\Delta t/2}-e^{-\gamma\Delta t/2}}-\left(s\left(\bar{\mathbf{u}}-\mathbf{u}_p\left(t+\frac{1}{2}\Delta t\right)\right)+s(1-s)\cdot\alpha\cdot\frac{\sum_{\gamma=1,6}\left(\bar{\rho}-\sum_{q=1,N_\gamma(t)}\rho_q\right)d\mathbf{n}^\gamma}{\sum_{q=1,N(t)}m_q}\right)\equiv\mathbf{u}_p(t+\frac{1}{2}\Delta t), \quad (19)$$

and

$$\mathbf{x}_p(t+\Delta t)=\mathbf{x}_p(t+\frac{1}{2}\Delta t)+\{\mathfrak{R}_2\}\cdot(1-s), \quad (20)$$

The hybrid scheme (17)-(20) has the following properties:

1. for s=0, which corresponds to the pure particulate phase, the algorithm reduces to the original stochastic leapfrog time integration scheme [29], which for small time steps and all-atom molecular dynamics further reduces to the standard deterministic Verlet-type time-integration scheme,

2. for s=1, which corresponds to the pure continuum hydrodynamic phase, the coarse-grained particles become passive tracers in the hydrodynamic field; in this case, the friction terms are retained to balance the stochastic excitation generated by the random fluctuation stress term of the LL-FH model in the absence of sufficient particle-particle interactions, while the stochastic particle excitation functions $\{\mathfrak{R}_1\}$ and $\{\mathfrak{R}_2\}$ are switched off to avoid double accounting.

## 3 Validation

### 3.1 Details of the numerical implementation

In the current implementation, following the model [19] the discrete particles are present in the entire computational domain. At the open boundaries, periodic boundary conditions are applied. The user-defined function $s=s(\mathbf{x},t)$ of the hybrid multiscale

model based on the two-phase analogy is specified so that it is zero in the centre of the computational domain and grows to the domain periphery where coarse-grained particles are driven by the external hydrodynamic field,

$$s(z)=\begin{cases} S_{\min}, & z \le R_{MD}; \\ \dfrac{z-R_{MD}}{R_{FH}-R_{MD}}\left(S_{\max}-S_{\min}\right)+S_{\min}, & R_{MD} < z < R_{FH}; \\ S_{\max}, & z \ge R_{FH}. \end{cases} \qquad (21)$$

where $R_{MD}$ and $R_{FH}$ are the radii of the discrete particle and the hydrodynamic zone which are user-defined parameters.

In comparison with the previous hybrid MD-FH model [19], which used the pure MD model in the entire subdomain region where $S = S_{\min}$, in the current AdResS-FH model the boundary of the $S = S_{\min}$ region corresponds to coarse-grained particles (fig.1).

In the rest of the AdResS region ($S = S_{\min}$), a smoothly varying weighting function is applied to separate the Coarse Grained (CG) region from the pure MD zone in the centre with a hybrid zone [31]:

$$w(z)=\begin{cases} 0, & z \ge R_{all-atom}+d_{hyb} \\ \cos^2\left(\dfrac{\pi}{2d_{hyb}}\left(z-d_{all-atom}\right)\right), & R_{all-atom}+d_{hyb} > z > R_{all-atom} \\ 1, & z \le R_{all-atom} \end{cases} \qquad (22)$$

where $R_{all-atom}$ and $d_{hyb}$ are the radius and the width of the all-atom MD and the hybrid zone, respectively, as defined by the user.

In Eqs. (21) and (22), $z=\sqrt{\left(x_1-L/2\right)^2+\left(x_2-L/2\right)^2+\left(x_3-L/2\right)^2}$ and $z = abs(x_1 - L/2)$ in case of the spherically symmetrical and one-dimensional s-

function distributions, respectively, where $L$ is the computation box size, the coordinate centre corresponds to the centre of the atomistic region, and the limiting values of the S-function used in the current implementation are: $S_{\min} = 0, S_{\max} = 0.98$.

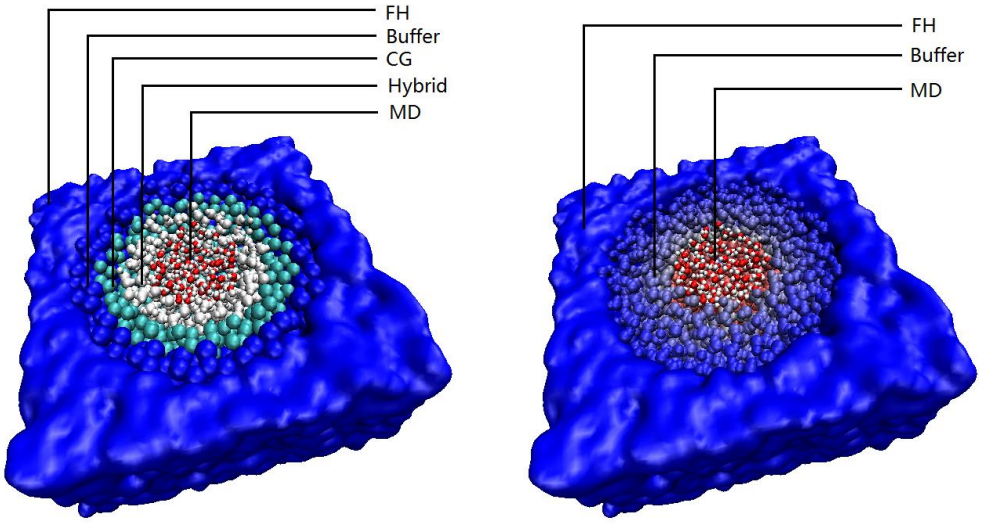


(a) (b)

**Figure 1**. Schematics of the domain decompositions of the current AdResS-FH (a) and the MD-FH model [19] (b). In the MD-FH model, the FH zone $(S \to 1)$ and MD zone $(S = 1)$ are connected by a buffer zone that is a mixture of MD and FH representations where variable S gradually changes from 0 to $S_{max}$. In the AdResS-FH model, inner pure MD zone is replaced by the AdResS model which consists of CG, hybrid (mixture of CG and MD), and MD sub-domains.

### 3.2 Test problems

A water system in equilibrium at standard stationary pressure and temperature

conditions is considered in a cubic box (7x7x7) $nm^3$. For solving the LL-FH equations (5)-(8), the computational domain is divided by a uniform computational grid corresponding to (5x5x5) control volumes (MD bins). All MD simulations are run in NVT ensemble with the standard Nose-Hover thermostat [32], [33]. For the AdResS-FH algorithm, the time constant for thermostat coupling is 0.5 ps. The MD integration time step is 2 fs, the integration time step of the hydrodynamic LL-FH model is 20 fs, and the total simulation time in all cases is 2 ns ($10^6$ time steps).

The same system is modelled with the suggested AdResS-FH method and with the original MD-FH method [19] for comparison.

In order to investigate sensitivity of the current triple-scale model to the choice of the thermostat in molecular dynamics, the tests of the AdResS-FH model have also been performed with the Berendsen thermostat. The model results with the Berendsen thermostat and those with the Nose-Hover thermostat are virtually the same. The lack of sensitivity to the thermostat details can be explained by the fact that the current one-way coupling implementation of the AdResS-FH does not take into account the feedback of AdResS particles on the hydrodynamic part of the model that is fixed.

For the first two test problems, a spherical distribution of the S-function is selected in each case so that $z=\sqrt{\left(x_1-L/2\right)^2+\left(x_2-L/2\right)^2+\left(x_3-L/2\right)^2}$ in Eqs (21) and (22). The size of the interior pure MD region ($R_{MD}$ in the MD-FH model and $R_{all-atom}$ in the AdResS model) is fixed the same for the different hybrid models to be compared.

There are two test cases considered: (1) the coordinate centre corresponding to the centre of the atomistic region is fixed at all times $\mathbf{x}_c\left(t\right)=0$ and (2) the coordinate

centre corresponding to the centre of the atomistic region oscillates about the origin in accordance with

$$\mathbf{x}_c(t) = \left(A \cdot \sin(\omega t), 0, 0\right), \tag{23}$$

where A=2 nm, $\omega = \pi/20$ rad/ps (see fig.2).

To analyse the solution accuracy of the hybrid multiscale models in cases 1 and 2, the radial distribution function (RDF) and the velocity autocorrelation function (VACF) of oxygen atoms are computed in the interior pure MD region. The results are compared with the solution of the classical all-atom MD simulation, which was performed in the same periodic box domain.

It can be remarked that problem 1 ("static case") is the standard consistency test for multi-resolution methods [31], [19]. In comparison with this, problem 2 ("dynamic case"), which to the best knowledge of the authors is considered here for the first time in the literature, is much more challenging. The apparent velocities and accelerations in the system are comparable to the thermal molecular fluctuations and the usual assumption of a scale separation that is typical of many multiscale models in the literature does not apply in this case. Consequently, any lack of balance in mass and momentum fluxes in the multiscale solution here would result in spurious velocities and accelerations in the results.

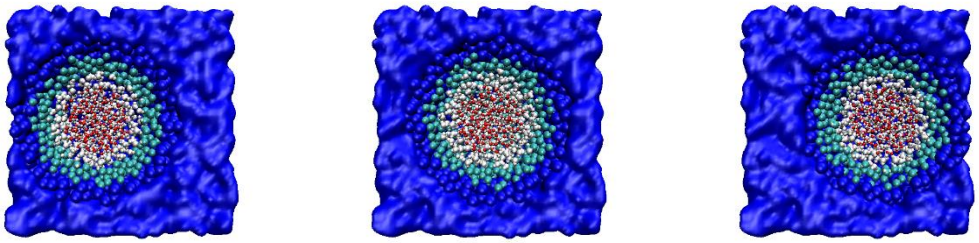

(a) (b) (c)

**Figure 2**. Schematic of the AdResS-FH model at $\omega t = -\pi/2$ (a), $\omega t = 0$ (b), $\omega t = \pi/2$ (c) for "dynamic" test 2.

Furthermore, to test sensitivity of the models to the size of the pure MD region that is one of the important numerical parameter which controls the model resolution, the simulations are performed for a few different values of $R_{all-atom}$ and $R_{MD}$ parameters of the AdResS-FH and the MD-FH model, respectively: $0.3\,(L/2)$ and $0.7\,(L/2)$. Other parameters of the two models are selected individually for best performance in each case. This results in two different configurations for the AdResS-FH model, 0.3-0.4-0.5-0.8 and 0.7-0.8-0.85-0.95, and two different configurations for the MD-FH model, 0.3-0.8 and 0.7-0.95. The two-digit notation for the MD-FH model corresponds to a set of $R_{MD}$ and $R_{FH}$ values in Eq (21).

For the AdResS-FH model, the first three of the four-digit notation correspond to a set of radial distances which control the distribution of the parameter w in the three layers of the AdResS model ( $R_{all-atom}, R_{all-atom} + d_{hyb}, R_{MD}$ ) in accordance with Eq (22), where S = 0, and the last one corresponds to the beginning of the hydrodynamic layer ( $R_{FH}$ ),

where S increases in Smax in accordance with Eq (21).

Figs. 3 and 4 compare the RDF and VACF solutions for oxygen for all four models with the reference distributions obtained from the all-atom MD simulation for problem 1 and 2, respectively.

For the “static” test 1, the AdResS-FH model shows consistently accurate results in an excellent agreement with the reference MD solution. In comparison with this, the accuracy of MD-FH model rather depends on the size of the inner MD domain zone as well as the width of the hybrid MD-FH zone.

For the “dynamic” test 2, the AdResS-FH model shows a very little sensitivity on the size of the pure MD region and its predictions are very close to the reference MD simulation again. In comparison with this, the MD-FH model for both sets of the selected parameters fails to predict the correct profile of the RDF function and its predictions of VACF become reasonable only when the size of the inner MD region is small so that the hybrid MD-FH zone is sufficiently large.

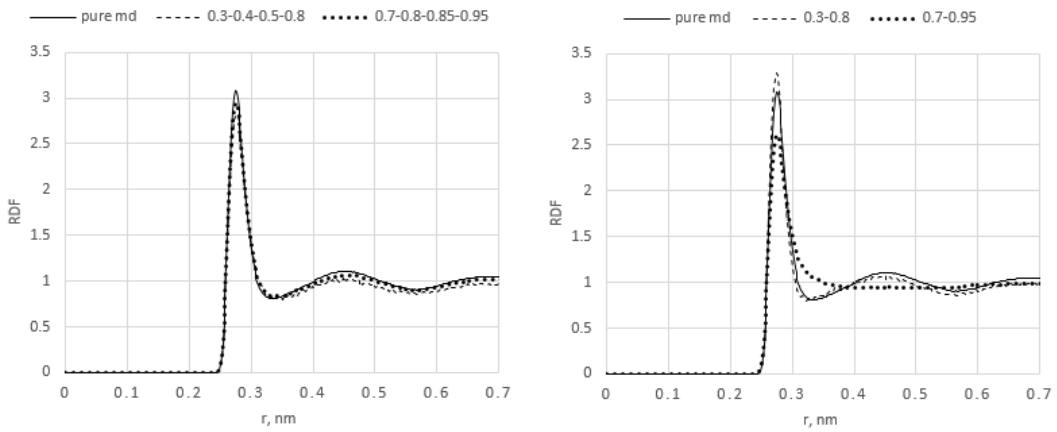


(a) (b)

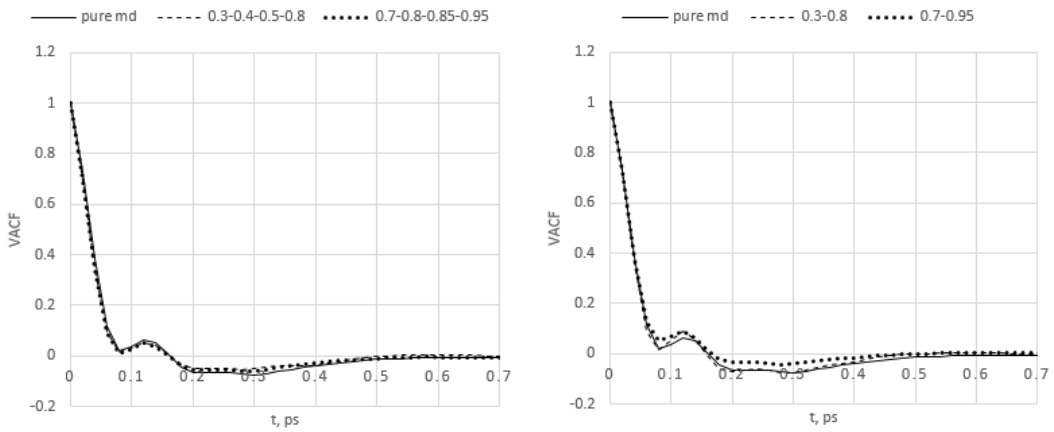


(c) (d)

**Figure 3**. Results of the "static" test 1: comparisons of the RDF and VACF distributions for oxygen atoms in the inner pure MD region for the AdResS-FH (a),(c) and MD-FH models (b),(d) for different sizes of the MD region.

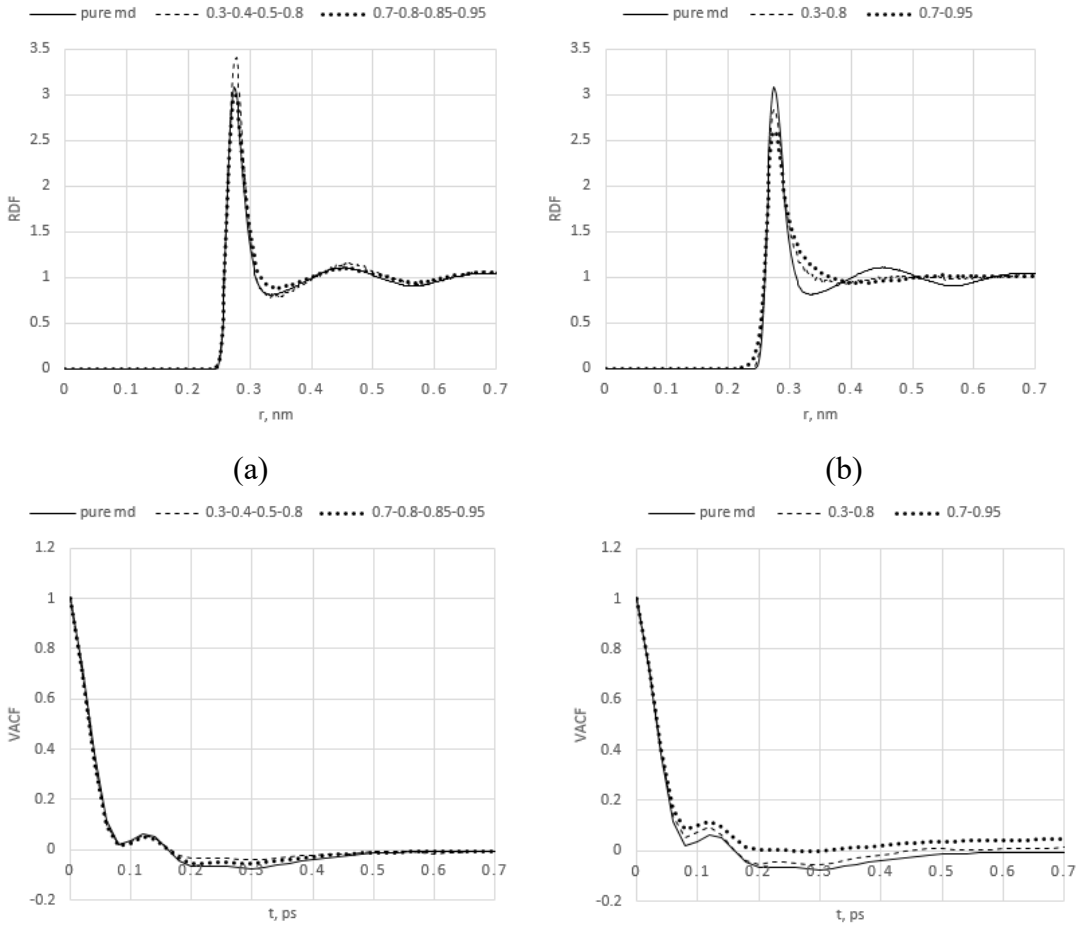


(a) (b)

(c) (d)

**Figure 4**. Results of the "dynamic" test 2: comparisons of the RDF and VACF

distributions for oxygen atoms in the inner pure MD region for the AdResS-FH (a),(c) and MD-FH models (b),(d) for different sizes of the MD region.

As discussed in the introduction, the larger error of the MD-FH method in comparison with the AdResS-FH scheme is due to a drastic change between the atom properties as they undergo a transition towards hydrodynamic particles. The hydrodynamic particles may come closer one to another compared to atoms in molecular dynamics. The less gradual transition between these two states leads to a non-negligible probability to find particles at a small distance between each other, hence, to large interatomic forces and an excursion from the correct equilibrium state of the system. This is illustrated in Fig. 5 which compares typical RDF solutions for oxygen for the stationary models obtained with AdReSs-FH and MD-FH methods in the entire computational domain including both the atomistic and the hydrodynamic zone. The size of the MD zone is set the same for both the methods and equal to 0.7 of the entire domain length. The centre of the MD zone is fixed which corresponds to conditions of the “static” test 1. The reference distribution obtained from the all-atom MD simulation in shown on the same plot for comparison. Note that, while the AdResS-FH solution captures the peak probability very closely compared to the reference MD solution, the peak of the MD-FH distribution looks somewhat diffused towards small interatomic distances. This means a nonzero probability of finding MD-FH particles closer to each other compared to the correct equilibrium distribution in molecular dynamics.

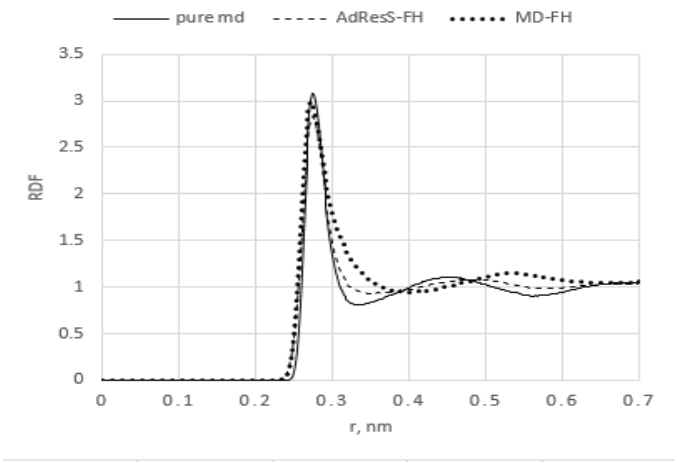


**Figure 5**. Comparison of the RDF profiles for oxygen atoms in the entire solution domain for the AdResS-FH and MD-FH model for the "static" test 1, which correspond to 0.7-0.8-0.85-0.95 and 0.7-0.95 hybrid domain configurations, respectively.

In addition to RDF and VACF, another important property of a hybrid model is capturing the correct level of thermal fluctuations of groups of atoms. Of particular interest is density and velocity fluctuations in the inner MD volume of the hybrid computational domain. Fig.6 compares the standard deviation (STD) of density and velocity of water atoms in the MD zone for the AdResS-FH and MD-FH models. The results correspond to the hardest, "dynamic" test 2 and the largest size of the inner MD zone (0.7 of the length of the entire computational box). The solutions of the two models correspond to 0.7-0.8-0.85-0.95 and 0.7-0.95 hybrid domain configurations, respectively. The reference profiles are obtained by running the all-atom MD simulations and extracting fluctuations for the same control volume size. These are shown on the same plots for comparison. The AdReS-FH prediction for the velocity

fluctuation are in an excellent agreement with the reference pure MD solution. In comparison with this, the velocity fluctuations of the MD-FH solution are notably amplified. The density fluctuations of the AdReS-FH solution show some 20% overprediction compared to the reference solution. For this quantity, the solution of the MD-FH method appears to be more accurate (within 10% error). The error of the AdReSs-FH solution for density can be explained by the sound speed effect. Indeed, the sound speed is well-known to affect the level of density fluctuations. But this quantity is not well preserved in the AdReSs scheme which has a correction to preserve the continuity of pressure across the hybrid zone but not that of the pressure derivative that defines the sound speed.

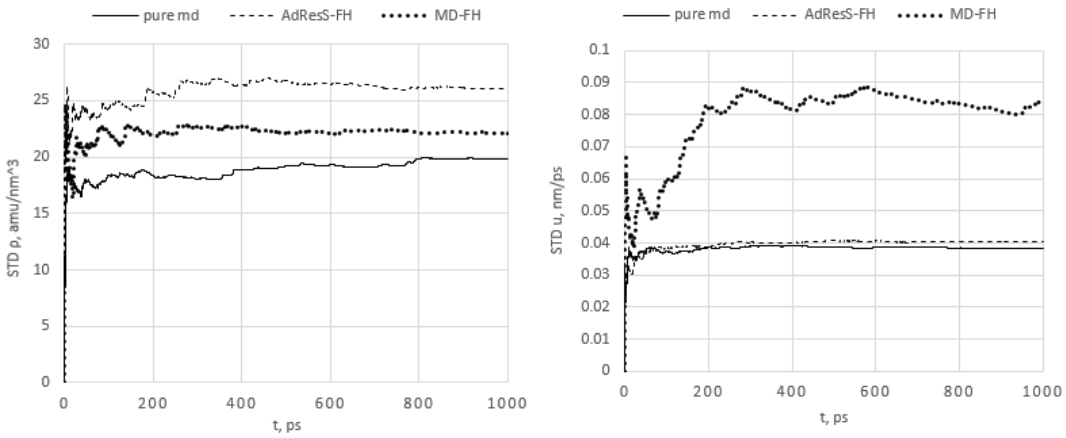


(a) (b)

Fig 6. Comparisons of the standard deviations of density (a) and velocity (b) fluctuations of the inner MD part of the AdResS-FH and MD-FH methods for conditions of the “dynamic” test 2 with the reference all-atom molecular dynamics solution.

Finally, accuracy of the new AdResS-FH model is tested for an acoustic wave

propagation problem following [21], [34] and [35]. In this case, coupling with macroscopic mass and momentum transfer is important and the problem cannot be solved by applying the pure AdResS method alone. Compared to the shear wave propagation test problems considered in [19] and [36] , acoustic wave propagation involves closely correlated fluctuations of density and velocity. Hence, it is a good test for both the macroscopic mass and the momentum conservation equations.

A normal high-frequency acoustic wave is specified in the same small computational box domain as considered for test problems 1 and 2. To simplify the boundary conditions, the acoustic wavelength is set equal to the domain size, L. The amplitude of the acoustic wave is 0.5% of the background values of pressure and density and is a few orders of magnitude smaller compared to the thermal fluctuations. Because of the scale separation, the acoustic wave influence on thermal fluctuations is neglected. Furthermore, due to the small size of the solution domain, the viscous dissipation effects on acoustic wave are ignored.

For numerical implementation, the acoustic wave is introduced into the background solution corresponding to no-flow conditions by modifying the underlying LL-FH solution so that

$$\begin{aligned} \bar{\rho} &= \rho^{FH} + \rho', \\ \bar{\mathbf{u}} &= \mathbf{u}^{FH} + \left(u_1', 0, 0\right), \end{aligned} \tag{24}$$

where $\rho' = \varepsilon \langle \rho \rangle \cos\left(\omega t - k x_1\right)$ and $u_1' = c_s \varepsilon \cos\left(\omega t - k x_1\right)$ are the solution of the corresponding linear wave propagation equation. The wavenumber is related to the

frequency via the dispersion relation so that $k = \frac{\omega}{c_s}$ where the phase velocity is equal to the sound speed $c_s = \sqrt{\frac{\partial P}{\partial \rho}}$ that is given in accordance with the isothermal equation of state for water, $P = P(\rho)$. $\left(\rho^{FH}, \mathbf{u}^{FH}\right)$ is the solution of the LL-FH equations (5)-(8) and $\langle \rho \rangle$ is the time-averaged (bulk-water) density value.

A high frequency wave case is selected so that $\omega / c_s$ is 0.897 rad/nm. This corresponds to a reduced frequency $\frac{\omega}{c_s}\Delta x = 4.398$ defined on the characteristic length scale of the problem, $\Delta x$ that is the width of the inner MD zone of the AdResS-FH model. Since $\frac{\omega}{c_s}\Delta x >> 1$ this amounts to an unsteady wave propagation regime.

Fig.7 shows how the AdResS-FH model is adapted for the acoustic wave propagation test by choosing a one-dimensional distribution function of the model parameters so that $z = abs(x_1 - L/2)$ in Eqs. (21),(22).

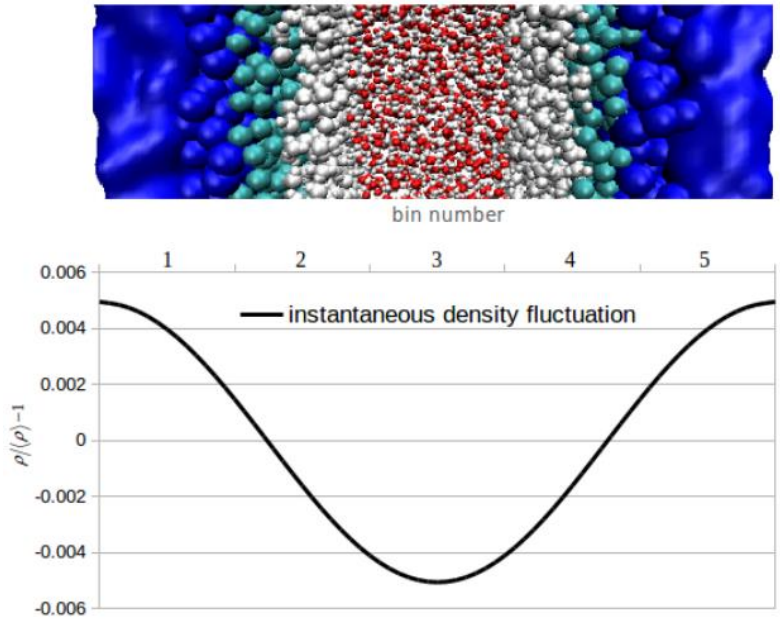

**Figure 7**. Schematic of the AdResS-FH model for the acoustic wave propagation test and a typical acoustic wave profile across the computational domain that is divided into (5x5x5) MD bins.

To analyse accuracy of the hybrid AdResS-FH model for this test, a numerical probe is placed in bin # 3 which corresponds to the pure MD region and the density time signal is calculated by averaging the contributions of all atoms in the bin.

It can be recalled that the acoustic signal to thermal noise ratio of the problem is very low, $O(10^{-2})$. However, the thermal noise fluctuations are not correlated in comparison with the small amplitude but strongly correlated acoustic signal that propagates in the $x_1$-direction. Therefore, in order to eliminate the thermal noise effect, the acoustic signal is first averaged along the homogeneous $x_2$ and $x_3$ directions and then phase averaged in accordance with the time period of the acoustic wave propagation, $t_0 = 2\pi/\omega$ over the window of about 1000 acoustic time periods.

Fig. 8 compares the resulting acoustic signal, which has been reconstructed in the pure MD region of the AdResS-FH model, with the analytical solution. A very good agreement both for the amplitude and the phase of the wave can be noted which confirms that the current implementation not only maintains a correct balance of mass and momentum without any significant acoustic wave dissipation but also accurately reproduces the phase velocity of the acoustic wave.

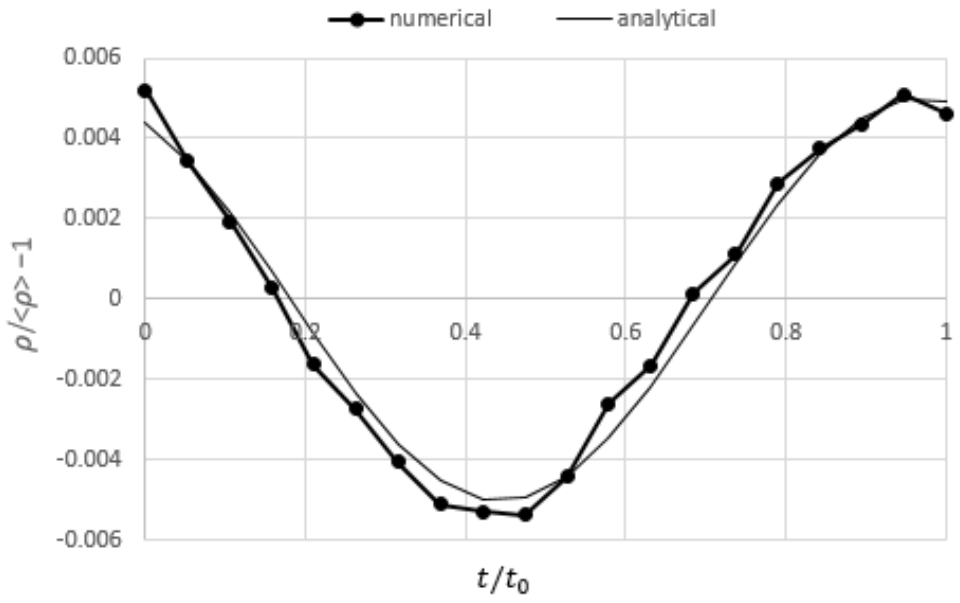


**Figure 8.** Acoustic wave propagation through the AdResS-FH domain: comparison of the density fluctuation obtained from the all-atom resolution part of the computational domain with the analytical solution.

## 4 Conclusions

A new multi-resolution scheme, which combines the scale-bridging AdResS method with Fluctuating Hydrodynamics (FH) is developed. In comparison with the existing modifications of AdResS in the literature, the current method is based on a state variable scheme which uses the analogy with two-hydrodynamics to smoothly connect the coarse-grained particles and continuum hydrodynamics as a particle and a continuous phase of the same liquid, respectively. The new model can also be considered as an extension of the previous Molecular Dynamics (MD)-FH coupling schemes based on the two-phase flow analogy to multi-resolution particle simulations. Thanks to this

extension, a more consistent transition between the MD region and the FH domain with a better control of inter particle distances has been achieved.

Numerical tests demonstrate that the suggested AdResS-FH model is more accurate and less sensitive to the key numerical parameters such as the width of the pure MD region compared to the previous MD-FH model. In particular, the new triple-scale model is shown to accurately reproduce the radial distribution function and the velocity auto-correlation of oxygen atoms for the challenging test case when the coordinate center of the hybrid region moves at high apparent velocities and accelerations so that the scale separation assumption does not apply. It is shown that the key improvement in accuracy of the new model compared to the "baseline" MD-FH model is associated with a more accurate preservation of correct inter particle distances in the entire computational domain including hydrodynamics. For the moving hybrid region test, the new AdResS-FH model also demonstrates an excellent accuracy in capturing the correct velocity fluctuations of the inner MD zone atoms as verified against the reference all-atom MD simulation. The density fluctuations of the same group of atoms are reproduced with a reasonable accuracy too despite the lack of preservation of correct sound speed across all layers of the AdResS model.

To analyse its accuracy for multiscale simulations of hydrodynamics flows, the AdResS-FH model is implemented for the problem of high frequency acoustic wave propagation in water and the results are compared with the analytical solution. It shown that the new model not only captures the correct amplitude of the acoustic wave without any significant amplitude attenuation but also accurately reproduces the phase velocity.

Future work will be devoted to extending the AdResS-FH model to a fully coupled approach where the hydrodynamic phase is computed on the fly from the MD solution by solving the governing equations (1)-(4) rather than the LL-FH equations (5)-(8) as well as keeping the coarse-grained particles in a small part of the continuum computational domain to speed up calculations. Other avenues for future work can include an extension of the suggested AdResS-FH approach to supramolecular coarse-grained (SCG) models, which map several molecules to one SCG particle, and which can be implemented by the use of dynamical mapping algorithm SWINGER [37] as well as combing the current approach with the AdResS- dissipative particle dynamics methods [38].

## 5 Acknowledgments

The work of JH was supported by China Scholarship Council (CSC). IK gratefully acknowledges the funding under the Marie Skłodowska-Curie Individual Fellowship Grant H2020-MSCA-IF-2015-700276 (HIPPOGRIFFE). This research utilised Queen Mary's Apocrita HPC facility, supported by QMUL Research-IT [39].

The authors are grateful to Dr Christoph Junghans for help with the AdResS model implementation in GROMACS version 4.6.7 [31] and Dr Dmitry Nerukh for helpful discussions on the two-phase flow analogy method.

## Appendix: Details of the stochastic excitation functions

In accordance with the integration method outlined in [29], several random variables are introduced:

$$U_t\left(\Delta t/2\right)=\frac{1}{m}\int_t^{t+\Delta t/2}e^{-\gamma(t+\Delta t/2-t')}R\left(t'\right)dt' \tag{A1}$$

$$X_{t+\Delta t/2}\left(\Delta t/2\right)=\frac{1}{m\gamma}\int_{t+\Delta t/2}^{t+\Delta t}\left(1-e^{-\gamma(t+\Delta t-t')}\right)R\left(t'\right)dt' \tag{A2}$$

The stochastic characteristics of $R\left(t'\right)$ are subjected to the same assumptions as in $\mathbf{R}_p$. In the SD leap-frog algorithm, the variables $\Re_1,\Re_2$ are defined so that

$$\left\{\Re_1\right\}=U_t\left(\Delta t/2\right)-e^{-\gamma\Delta t}U_t\left(-\Delta t/2\right)+O\left[\left(\Delta t\right)^3\right] \tag{A3}$$

$$\left\{\Re_2\right\}=X_{t+\Delta t/2}\left(\Delta t/2\right)-X_{t+\Delta t/2}\left(-\Delta t/2\right)+O\left[\left(\Delta t\right)^3\right] \tag{A4}$$

$U_t\left(-\Delta t/2\right)$ and $X_{t-\Delta t/2}\left(\Delta t/2\right)$ are integrals of $R\left(t\right)$ over the same time interval $(t_n,t_{n+1/2})$ and defined by：

$$U_t\left(-\Delta t/2\right)=\frac{1}{m}\int_{t-\Delta t/2}^{t}(-)e^{-\gamma(t-\Delta t/2-t')}R\left(t'\right)dt' \tag{A5}$$

and

$$X_{t-\Delta t/2}\left(\Delta t/2\right)=\frac{1}{m\gamma}\int_{t-\Delta t/2}^{t}\left(1-e^{-\gamma(t-t')}\right)R\left(t'\right)dt' \tag{A6}$$

These variables are correlated with each other.
The other pair of random variables is defined in a similar way:

$$X_{t+\Delta t/2}\left(-\Delta t/2\right)=\frac{1}{m\gamma}\int_{t}^{t+\Delta t/2}(-)\left(1-e^{-\gamma(t-t')}\right)R\left(t'\right)dt' \tag{A7}$$

and

$$U_t\left(\Delta t/2\right)=\frac{1}{m}\int_t^{t+\Delta t/2}e^{-\gamma(t+\Delta t/2-t')}R\left(t'\right)dt' \tag{A8}$$

Both pairs of random variables are subjected to a bivariate Gaussian probability distribution [40]. For the first pair of random variables:

$$W\left(X_{t-\Delta t/2}\left(\Delta t/2\right),U_t\left(-\Delta t/2\right)\right)=\left[4\pi^2\sigma_1^2\sigma_2^2\left(1-k^2\right)\right]^{-1/2}e^{-\left[\sigma_2^2X_{t-\Delta t/2}^2\left(\Delta t/2\right)-2\sigma_1\sigma_2kX_{t-\Delta t/2}\left(\Delta t/2\right)U_t\left(-\Delta t/2\right)+\sigma_1^2U_t^2\left(-\Delta t/2\right)\right]/\left[2\sigma_1^2\sigma_2^2\left(1-k^2\right)\right]} \tag{A9}$$

Here the parameters $\sigma_1$, $\sigma_2$ and $k$ are determined from the calculation of

$\left\langle X^2_{t-\Delta t/2}(\Delta t/2)\right\rangle$, $\left\langle U_t^2(-\Delta t/2)\right\rangle$, and $\left\langle X_{t-\Delta t/2}(\Delta t/2)U_t(-\Delta t/2)\right\rangle$, and the property of the stochastic forces

$$\left\langle R(t)R(t')\right\rangle = 2m\gamma k_B T_{ref}\delta(t-t') \tag{A10}$$

Here $k_B$ is the Boltzmann constant and $T_{ref}$ is the reference temperature.

The rest of the parameters used are defined below:

$$\sigma_1^2 = \left\langle X^2_{t-\Delta t/2}(\Delta t/2)\right\rangle = \frac{k_B T_{ref}}{m\gamma^2} C(\gamma\Delta t/2) \tag{A11}$$

$$\sigma_2^2 = \left\langle U_t^2(-\Delta t/2)\right\rangle = \frac{k_B T_{ref}}{m}\left(e^{\gamma\Delta t}-1\right) \tag{A12}$$

$$k\sigma_1\sigma_2 = \left\langle X_{t-\Delta t/2}(\Delta t/2)U_t(-\Delta t/2)\right\rangle = \frac{k_B T_{ref}}{m\gamma} D(\gamma\Delta t/2) \tag{A13}$$

$$\sigma_2^2\left(1-k^2\right) = \sigma_2^2 - \left(k\sigma_1\sigma_2\right)^2/\sigma_1^2 = \frac{k_B T_{ref}}{m} B(\gamma\Delta t/2)/C(\gamma\Delta t/2) \tag{A14}$$

and

$$k\sigma_2/\sigma_1 = \left(k\sigma_1\sigma_2\right)/\sigma_1^2 = \gamma D(\gamma\Delta t/2)/C(\gamma\Delta t/2) \tag{A15}$$

where

$$C(\gamma\Delta t/2) = \gamma\Delta t - 3 + 4e^{-\gamma\Delta t/2} - e^{-\gamma\Delta t} \tag{A16}$$

$$D(\gamma\Delta t/2) = 2 - e^{\gamma\Delta t/2} - e^{-\gamma\Delta t/2} \tag{A17}$$

and

$$B(\gamma\Delta t/2) = \gamma\Delta t\left(e^{\gamma\Delta t}-1\right) - 4\left(e^{\gamma\Delta t/2}-1\right)^2 \tag{A18}$$

For the second pair of random variables, the bivariate Gaussian probability distribution reads

$$W\left(U_t(\Delta t/2), X_{t+\Delta t/2}(-\Delta t/2)\right) = \left[4\pi^2\rho_1^2\rho_2^2\left(1-q^2\right)\right]^{-1/2} e^{-\left[\rho_2^2 U_t^2(\Delta t/2) - 2\rho_1\rho_2 q U_t(\Delta t/2)X_{t+\Delta t/2}(-\Delta t/2) + \rho_1^2 X_{t+\Delta t/2}(-\Delta t/2)\right]/\left[2\rho_1^2\rho_2^2\left(1-q^2\right)\right]} \tag{A19}$$

The parameters $\rho_1$, $\rho_2$ and $q$ are determined from the calculation of $\left\langle U_t^2\left(\Delta t/2\right)\right\rangle$, $\left\langle X_{t+\Delta t/2}^2\left(-\Delta t/2\right)\right\rangle$, $\left\langle U_t\left(\Delta t/2\right)X_{t+\Delta t/2}\left(-\Delta t/2\right)\right\rangle$, and using the expression (A10) so that:

$$\rho_1^2=\left\langle U_t^2\left(\Delta t/2\right)\right\rangle=\frac{k_BT_{ref}}{m}(-)\left(e^{-\gamma\Delta t}-1\right) \tag{A20}$$

$$\rho_2^2=\left\langle X_{t+\Delta t/2}^2\left(-\Delta t/2\right)\right\rangle=\frac{k_BT_{ref}}{m\gamma^2}(-)C(-\gamma\Delta t/2) \tag{A21}$$

$$q\rho_1\rho_2=\left\langle U_t\left(\Delta t/2\right)X_{t+\Delta t/2}\left(-\Delta t/2\right)\right\rangle=\frac{k_BT_{ref}}{m\gamma}(-)D(-\gamma\Delta t/2) \tag{A22}$$

$$\rho_2^2\left(1-q^2\right)=\rho_2^2-\left(q\rho_1\rho_2\right)^2/\rho_1^2=\frac{k_BT_{ref}}{m\gamma^2}(-)B(-\gamma\Delta t/2)/\left(e^{-\gamma\Delta t}-1\right) \tag{A23}$$

and

$$q\rho_2/\rho_1=\left(q\rho_1\rho_2\right)/\rho_1^2=\gamma^{-1}D(-\gamma\Delta t/2)/\left(e^{-\gamma\Delta t}-1\right) \tag{A24}$$

**References**


[1] T. R. Teschner, L. Könözsy, and K. W. Jenkins, “Progress in particle-based multiscale and hybrid methods for flow applications,” *Microfluidics and Nanofluidics*, vol. 20, no. 4, 2016.

[2] P. Español, P. B. Warren, and P. B. Warren, “Perspective : Dissipative particle dynamics,” *J. Chem. Phys.*, vol. 150901, 2017.

[3] R. Delgado-Buscalioni and P. V. Coveney, “Continuum-particle hybrid coupling for mass, momentum, and energy transfers in unsteady fluid flow,” *Physical Review E - Statistical Physics, Plasmas, Fluids, and Related Interdisciplinary Topics*, vol. 67, no. 4, p. 13, 2003.

[4] R. A. Gingold and J. J. Monaghan, “Smoothed particle hydrodynamics: theory and application to non-spherical stars,” *Monthly Notices of the Royal Astronomical Society*, vol. 181, no. 3, pp. 375–389, 1977.

[5] L. B. Lucy, “A numerical approach to the testing of the fission hypothesis,” *Astronomical Journal*, vol. 82, pp. 1013–1024, Dec. 1977.

[6] P. L. Bhatnagar, E. P. Gross, and M. Krook, “A Model for Collision Processes in Gases. I. Small Amplitude Processes in Charged and Neutral One-Component Systems,” *Phys. Rev.*, vol. 94, no. 3, pp. 511–525, May 1954.

[7] S. Chen and G. D. Doolen, “Lattice Boltzmann method for fluid flows,” *Annual Review of Fluid Mechanics*, vol. 30, no. 1, pp. 329–364, 1998.

[8] O. Pironneau, “Finite element method for fluid,” vol. 1988, p. 176, 1988.

[9] M. J. Turner, R. W. Clough, H. C. Martin, and L. J. Topp, “Journal of the Aeronautical Sciences,” *Journal Of The Aeronautical Sciences*, vol. 40, no. 6, pp. 145–160, 2003.

[10] G. R. Liu and S. S. Quek, Eds., “The Finite Element Method,” in *The Finite Element Method (Second Edition)*, Second Edi., Oxford: Butterworth-Heinemann, 2014, p. i-.

[11] H. K. Versteeg and W. Malalasekera, *An Introduction to computational fluid dynamics*, vol. M. 2007.

[12] S. T. O’Connell and P. A. Thompson, “Molecular dynamics-continuum hybrid computations: A tool for studying complex fluid flows,” *Physical Review E*, vol. 52, no. 6, pp. 5792–5795, 1995.

[13] N. G. Hadjiconstantinous and A. T. Patera, “Heterogeneous Atomistic-Continuum Representations for Dense Fluid Systems,” *International Journal of Modern Physics C - IJMPC*, vol. 8, pp. 967–976, 1997.

[14] X. B. Nie, S. Y. Chen, W. N. E, and M. O. Robbins, “A continuum and molecular dynamics hybrid method for micro- and nano-fluid flow,” *Journal of Fluid Mechanics*, vol. 500, pp. 55–64, 2004.

[15] E. G. Flekkøy, G. Wagner, and J. Feder, “Hybrid model for combined particle and continuum dynamics,” *EPL (Europhysics Letters)*, vol. 52, no. 3, p. 271, 2000.

[16] J. H. Walther, M. Praprotnik, E. M. Kotsalis, and P. Koumoutsakos, “Multiscale simulation of water flow past a C540 fullerene,” *Journal of Computational Physics*, vol. 231, no. 7. pp. 2677–2681, 2012.

[17] M. Praprotnik, L. Delle Site, and K. Kremer, “Adaptive resolution molecular-dynamics simulation: Changing the degrees of freedom on the fly,” *Journal of Chemical Physics*, vol. 123, no. 22, 2005.

[18] A. Markesteijn, S. Karabasov, A. Scukins, D. Nerukh, V. Glotov, and V. Goloviznin, “Concurrent multiscale modelling of atomistic and hydrodynamic processes in liquids,” *Philosophical Transactions of the Royal Society A: Mathematical, Physical and Engineering Sciences*, vol. 372, no. 2021, pp. 20130379–20130379, 2014.

[19] I. Korotkin, S. Karabasov, D. Nerukh, A. Markesteijn, A. Scukins, and V. Farafonov, “A hybrid molecular dynamics/fluctuating hydrodynamics method

for modelling liquids at multiple scales in space and time," *Journal of Chemical Physics*, vol. 143, no. 1, 2015.

[20] R. Delgado-Buscalioni and P. V. Coveney, "USHER: An algorithm for particle insertion in dense fluids," *Journal of Chemical Physics*, vol. 119, no. 2, pp. 978–987, 2003.

[21] R. Delgado-Buscalioni, K. Kremer, and M. Praprotnik, "Concurrent triple-scale simulation of molecular liquids," *Journal of Chemical Physics*, vol. 128, no. 11, 2008.

[22] L. D. Landau and E. M. Lifshitz, *Statistical physics. Part 1*. Amsterdam; London: Elsevier Butterworth Heinemann, 1980.

[23] A. P. Markesteijn, S. A. Karabasov, V. Y. Glotov, and V. M. Goloviznin, "A new non-linear two-time-level Central Leapfrog scheme in staggered conservation–flux variables for fluctuating hydrodynamics equations with GPU implementation," *Computer Methods in Applied Mechanics and Engineering*, vol. 281, pp. 29–53, Nov. 2014.

[24] I. Korotkin, D. Nerukh, E. Tarasova, V. Farafonov, and S. Karabasov, "Two-phase flow analogy as an effective boundary condition for modelling liquids at atomistic resolution," *Journal of Computational Science*, vol. 17, pp. 446–456, Nov. 2016.

[25] E. Tarasova, I. Korotkin, V. Farafonov, S. Karabasov, and D. Nerukh, "Complete virus capsid at all-atom resolution: Simulations using molecular dynamics and hybrid molecular dynamics/hydrodynamics methods reveal semipermeable

membrane function," *Journal of Molecular Liquids*, 2017.

[26] L. Verlet, "Computer 'Experiments' on Classical Fluids. I. Thermodynamical Properties of Lennard-Jones Molecules," *Phys. Rev.*, vol. 159, no. 1, pp. 98–103, Jul. 1967.

[27] S. Poblete, M. Praprotnik, K. Kremer, and L. D. Site, "Coupling different levels of resolution in molecular simulations," *The Journal of Chemical Physics*, vol. 132, no. 11, p. 114101, 2010.

[28] S. Fritsch, S. Poblete, C. Junghans, G. Ciccotti, L. Delle Site, and K. Kremer, "Adaptive resolution molecular dynamics simulation through coupling to an internal particle reservoir," *Phys. Rev. Lett.*, vol. 108, no. 17, p. 170602, Apr. 2012.

[29] W. F. van Gunsteren and H. J. C. Berendsen, "A leap frog algorithm for stochastic dynamics," *Molecular Simulation*, vol. 1, no. May 2013, pp. 173–185, 1988.

[30] D. van der Spoel, E. Lindahl, and B. Hess, *GROMACS User Manual version 4.6.7*. 2014.

[31] H. J. C. Berendsen, D. van der Spoel, and R. van Drunen, "GROMACS: A message-passing parallel molecular dynamics implementation," *Computer Physics Communications*, vol. 91, no. 1, pp. 43–56, 1995.

[32] S. Nosé, "A unified formulation of the constant temperature molecular dynamics methods," *The Journal of Chemical Physics*, vol. 81, no. 1, pp. 511–519, 1984.

[33] W. G. Hoover, "Canonical dynamics: Equilibrium phase-space distributions," *Phys. Rev. A*, vol. 31, no. 3, pp. 1695–1697, Mar. 1985.

[34] G. De Fabritiis, R. Delgado-Buscalioni, and P. V. Coveney, “Multiscale modeling of liquids with molecular specificity,” *Physical Review Letters*, vol. 97, no. 13, pp. 1–4, 2006.

[35] R. Delgado-Buscalioni, K. Kremer, and M. Praprotnik, “Coupling atomistic and continuum hydrodynamics through a mesoscopic model: Application to liquid water,” *Journal of Chemical Physics*, vol. 131, no. 24, pp. 1–8, 2009.

[36] R. Delgado-Buscalioni and G. De Fabritiis, “Embedding molecular dynamics within fluctuating hydrodynamics in multiscale simulations of liquids,” *Physical Review E - Statistical, Nonlinear, and Soft Matter Physics*, vol. 76, no. 3, pp. 1–13, 2007.

[37] J. Zavadlav, S. J. Marrink, and M. Praprotnik, “Multiscale simulation of protein hydration using the SWINGER dynamical clustering algorithm,” *Journal of Chemical Theory and Computation*, p. acs.jctc.7b01129, 2018.

[38] J. Zavadlav and M. Praprotnik, “Adaptive resolution simulations coupling atomistic water to dissipative particle dynamics,” *Journal of Chemical Physics*, vol. 147, no. 11, 2017.

[39] T. King, S. Butcher, and L. Zalewski, “Apocrita - High Performance Computing Cluster for Queen Mary University of London,” Mar. 2017.

[40] A. Papoulis, *Probability, Random Variables and Stochastic Processes*. New York: McGraw-Hil, 1965.